Published in final edited form as:
J Biomed Opt. 2008 ; 13(5): 054019. doi:10.1117/1.2982524.

Double-layer estimation of intra- and extracerebral hemoglobin concentration with a time-resolved system

Louis Gagnon, **Claudine Gauthier**, **Rick D. Hoge**, and **Frédéric Lesage**
Institut de Génie Biomédical, École Polytechnique de Montréal, C.P. 6079, succ. Centre-Ville, Montréal, Québec H3C 3A7, Canada

Louis Gagnon: louis-2.gagnon@polymtl.ca; Claudine Gauthier: ; Rick D. Hoge: ; Frédéric Lesage:

Juliette Selb and **David A. Boas**
Massachusetts General Hospital, Athinoula A. Martinos Center for Biomedical Imaging, Charlestown, Massachusetts 02129

Abstract

We present *in vivo* measurements of baseline physiology from five subjects with a four-wavelength (690, 750, 800, and 850 nm) time-resolved optical system. The measurements were taken at four distances: 10, 15, 25, and 30 mm. All distances were fit simultaneously with a two-layered analytical model for the absorption and reduced scattering coefficient of both layers. The thickness of the first layer, comprising the skin, scalp, and cerebrospinal fluid, was obtained from anatomical magnetic resonance images. The fitting procedure was first tested with simulations before being applied to *in vivo* measurements and verified that this procedure permits accurate characterization of the hemoglobin concentrations in the extra- and intracerebral tissues. Baseline oxyhemoglobin, deoxyhemoglobin, and total hemoglobin concentrations and oxygen saturation were recovered from *in vivo* measurements and compared to the literature. We observed a noticeable intersubject variability of the hemoglobin concentrations, but constant values for the cerebral hemoglobin oxygen saturation.

Keywords

Biomedical optics; reflectance; optical properties

1 Introduction

Imaging with near-infrared diffuse optical imaging (DOI) in the neurosciences has seen increased interest over the past 15 years.[1–4] In the commonly used continuous-wave (CW) version,[5,6] DOI can only measure relative changes in oxy-(HbO_2) and deoxyhemoglobin (HbR) concentrations. On the contrary, frequency domain (FD)[7–10] and time domain (TD)[11–19] technologies enable absolute measurements of the medium's optical properties.[20–22] This is particularly useful to calibrate brain activation and quantify the underlying hemodynamic processes within the brain. For example, multimodal studies (e.g., optical-MRI fusion[23]) need quantitative information to estimate the cerebral metabolic rate of oxygen ($CMRO_2$). In addition, the blood-oxygen level dependant (BOLD) signal depends both on cerebral blood flow (CBF) and $CMRO_2$. However, this relation is not straightforward, and a

Address all correspondence to: Louis Gagnon, Institut de Génie Biomédical, École Polytechnique de Montréal, C.P. 6079, succ. Centre-Ville, Montréal, Québec H3C 3A7, Canada; E-mail: E-mail: louis-2.gagnon@polymtl.ca.

calibration constant must be estimated. The change in CBF can be measured separately by arterial spin labeling fMRI so the only two unknowns are the calibration constant and $CMRO_2$. To estimate $CMRO_2$, one must measure the BOLD signal at two different CBF values but without altering the $CMRO_2$. This must be done during hypercapnic periods using two different levels of CO_2 pressure.[24] However, TD measurements could provide an alternative to this procedure.

Brain optical properties have been measured previously *in vitro*,[25] but physiological factors make those measurements distinct from the *in vivo* situation. Among those distinctions is the swelling of the mitochondria, which results in structural changes, and the small fluctuations of the brain temperature, which change the hemoglobin solubility in the blood. Moreover, previous studies performing *in vivo* measurements reported noticable intersubject variability.[8,26] These results preclude the generalization of single-subject measured values to other subjects and confirm the importance of obtaining these values individually for quantitative imaging.

In previous work, baseline optical measurements with a TD system using multidistances and a homogeneous model has been used to fit the data and estimate the optical parameters.[26,27] A major drawback is that this homogeneous model does not distinguish between hemoglobin concentrations in the scalp and those of the cerebral tissues, because it does not account for the layered structure of the head. The superficial layer, the skin and skull, limit the accuracy of DOI, since light is also absorbed and scattered in these regions, which are not part of the cerebral cortex. Moreover, the skin layer is subject to a physiology that may cause interference in the process of recovering cerebral activity. Several methods based on multi-distance measurements have been developed to overcome this problem.[28–31] In a multimodal study combining position emission tomography and TD optical imaging, it was shown that the contributions from these superficial layers are reduced significantly, even using a homogeneous model, when source-detector distances are increased beyond 4 cm.[32] Such measurements require a large signal-to-noise ratio, which was not available with the system used in our experiment.

Separately, analytical models have been developed by solving the diffusion equation and its boundary conditions for a two-layered medium.[22,33–35] These models, validated with Monte Carlo simulations, showed adequate efficiencies at recovering the parameters if the thickness of the first layer of the model was known *a priori*. *In vivo* measurements with a two-layered model also have been reported using a FD system,[8] and as expected, clear distinctions between scalp and cerebral tissues properties were made. The goal here is to provide further confirmation of the above FD results (Choi et al.) with an independent TD technique.

In this work, we report intra- and extracerebral hemoglobin concentrations recovered on individual subjects with a time-resolved system using a two-layered analytical model for the first time. The measurements were taken with four wavelengths (690, 750, 800, and 850 nm) at four distances: 10, 15, 25, and 30 mm. All wavelengths were fit simultaneously with a two-layered analytical model for the absorption and reduced scattering coefficient of both layers. Concentrations were then computed with the recovered absorption coefficients. We observed a large variability between subjects. Results were compared to the literature, and differences between time and frequency measurements for the oxygen saturation in the skin and skull layer were observed.

2 Theory

Light propagation in a turbid medium is described by the radiative transport equation. This equation can be further approximated by the diffusion equation when the medium is highly scattering. Analytical solutions have been developed in the literature for simple geometries

and homogeneous media.[36] Analytical[35,37–46] and numerical[33,47] solutions also have been developed for multilayered media. Only the solutions used in our fitting procedure are described in this section.

2.1 Homogenous Medium

As given in Kienle et al.,[33] the radiance at the surface of a homogeneous medium at a distance ρ from the photon source following a time *t* after the source pulse is given by

$$R(\rho,t)=0.118\Phi(\rho,z=0,t)+0.306\left.\frac{\partial\Phi}{\partial z}\right|_{z=0}, \tag{1}$$

where Φ is the solution of the diffusion equation given by Patterson et al.[36] with an extrapolated boundary condition,[48] and Φ is expressed as

$$\Phi(\rho,z,t)=\frac{Ac}{(4\pi Dct)^{3/2}}\exp(-\mu_a ct)\left\{\exp\left[-\frac{z_-^2}{4Dct}\right]-\exp\left[-\frac{z_*^2}{4Dct}\right]\right\}, \tag{2}$$

where c=0.214 mms^{-1} is the speed of light in tissue, and A is an amplitude factor accounting for the source magnitude. The diffusion coefficient, D, is defined by

$$D=\frac{1}{3[\mu_a+\mu_s']^{-1}}, \tag{3}$$

where μ_a is the absorption coefficient, and μ_s' is the effective scattering coefficient. Also, $z_-^2=z_0^2+\rho^2$ is the distance between the isotropic photon source and the detector, and $z_*^2=(z_0+2z_b)^2+\rho^2$ is the distance between the negative imaginary sources and the detector, where $z_0=1/\mu_s'$ and z_b is defined by

$$z_b=\frac{1+R_{\text{eff}}}{1-R_{\text{eff}}}2D_1. \tag{4}$$

Following Ref. 48, R_{eff} represents the fraction of photons that are internally diffusely reflected at the boundary and is assumed to be 0.493 for a refractive index of 1.4 in tissue.

An estimation of the absorption coefficient can be made using the Neumann boundary condition:[36]

$$\lim_{t\to\infty}\frac{d}{dt}\log_e R(\rho,t)=-\mu_a c. \tag{5}$$

One can then use a linear regression on the tail of the logarithm of the reflectance to estimate μ_a.

2.2 Two-Layered Medium

For a two-layer medium, the radiance is again given by Eq. (1), but this time Φ is the solution of the diffusion equation for a two-layer medium under the extrapolated boundary condition.[22,33,34] The expression in the first layer is given in the Fourier domain by

$$\phi_1(z,s,\omega)=\frac{\sinh[\alpha_1(z_b+z_0)]}{D_1\alpha_1}\times\frac{D_1\alpha_1\cosh[\alpha_1(\ell-z)]+D_2\alpha_2\sinh[\alpha_1(\ell-z)]}{D_1\alpha_1\cosh[\alpha_1(\ell+z_b)]+D_2\alpha_2\sinh[\alpha_1(\ell+z_b)]}-\frac{\sinh[\alpha_1(z_0-z)]}{D_1\alpha_1}\quad\text{for } 0\le z\le z_0, \tag{6}$$

Where $\alpha_1^2=(D_1s^2+\mu_{a1}+i\omega/c)/D_1$, and s is the radial spatial frequency.

The spatial Fourier inversions, over s, must be done numerically, because no analytical solutions are available. To avoid numerical errors, hyperbolic functions in Eq. (6) are expanded. Because we assume cylindrical symmetry of the problem, the two-dimensional Fourier inversion of the preceding expression is given by

$$\Phi^{\omega}(\rho,s,\omega)=\frac{A}{2\pi}\int_0^{\infty}\mathrm{d}s\phi_1(s,z,\omega)sJ_0(s\rho), \tag{7}$$

where J_0 is the Bessel function of zeroth order, and A is an amplitude factor as described previously. The Hankel transform in Eq. (7) is done numerically by using a Gauss-Laguerre quadrature of 5000 points. The nodes and the weights are calculated with MATLAB using the algorithm presented in Ref. 49. To obtain the TD reflectance, one must calculate the real and the imaginary part of

$$R(\rho,\omega)=0.118\Phi^{\omega}(\rho,z=0,\omega)+0.306\left.\frac{\partial\Phi^{\omega}}{\partial z}\right|_{z=0} \tag{8}$$

for a set of frequencies, then perform a fast Fourier transform.

2.3 Hemoglobin Concentration Recovery

We are interested in recovering hemoglobin concentrations. By assuming that oxy- and deoxyhemoglobin, as well as water, are the dominant absorbers between 690 and 850 nm in tissue, and ignoring other background absorbers,[32,50–52] one can construct the following linear system:

$$\begin{bmatrix}\mu_a(\lambda_1)\\ \mu_a(\lambda_2)\\ \mu_a(\lambda_3)\\ \mu_a(\lambda_4)\end{bmatrix}=\begin{bmatrix}\varepsilon_{\mathrm{HbO_2}}(\lambda_1) & \varepsilon_{\mathrm{HbR}}(\lambda_1) & \varepsilon_{\mathrm{H_2O}}(\lambda_1)\\ \varepsilon_{\mathrm{HbO_2}}(\lambda_2) & \varepsilon_{\mathrm{HbR}}(\lambda_2) & \varepsilon_{\mathrm{HO_2}}(\lambda_2)\\ \varepsilon_{\mathrm{HbO_2}}(\lambda_3) & \varepsilon_{\mathrm{HbR}}(\lambda_3) & \varepsilon_{\mathrm{H_2O}}(\lambda_3)\\ \varepsilon_{\mathrm{HbO_2}}(\lambda_4) & \varepsilon_{\mathrm{HbR}}(\lambda_4) & \varepsilon_{\mathrm{H_2O}}(\lambda_4)\end{bmatrix}\begin{bmatrix}C_{\mathrm{HbO_2}}\\ C_{\mathrm{HbR}}\\ C_{\mathrm{H_2O}}\end{bmatrix}. \tag{9}$$

In this work, we assumed 70% of water for both the superficial tissues and the brain.[32] The system was thus reduced to four equations and two unknowns and was overdetermined. The hemoglobin concentrations were recovered by inverting Eq. (9) with a least-square fit. The extinction coefficients $\in(\lambda)$ can be found in the literature[53,54] while $\mu_a(\lambda)$ were recovered from the measurements.

3 Methodology

A system consisting of four pulsed lasers (PicoQuant, Berlin, Germany) operating at 690, 750, 800, and 850 nm, and four single-photon counting photomultiplier tubes (PMTs), was used to collect the light. A 4:1 combiner temporally interlaced the four wavelengths in a single fiber. Four detection fibers were placed at 10, 15, 25, and 30 mm, respectively, from the source fiber on a rubber patch. The latter was then placed on the forehead of the subject. Measurements were taken for both the left and right hemisphere. Photons were collected for a period of 300 seconds to generate sufficient statistics, i.e., a total count of more than 10^4 photons.

Five healthy adult subjects were recruited for this experiment. Every one previously passed a magnetic resonance imaging (MRI) exam (Siemens MAGNETOM Trio 3T, Malvern, Pennsylvania). We used the anatomical T1 image to measure the thickness of the scalp, skull, and cerebrospinal fluid (CSF) layers with the software SPM5 (UCL, London, UK). For the optical measures, the subjects were seated on a comfortable chair and were asked to stay calm during the acquisition. The experiment took place in a dark room to reduce the noise on the PMTs.

The fitting procedure used a nonlinear optimization routine (MATLAB function *lsqcurvefit*) with parameters μ_a, μ_s, and the amplitude factor A to get the best fit of the theoretical model to the experimental temporal point spread functions (TPSFs). The 16 TPSFs (four distances and four wavelengths) were first fit individually with a homogeneous model, Eq. (1) and Eq (2), with three parameters: μ_a, μ_s, and the amplitude factor A. The TPSFs were then fit simultaneously four by four (four distances for each wavelength) using the two-layered model, Eq. (6)– Eq (8), using eight parameters (μ_a and μ_s for each layer and an amplitude factor for each TPSF). For each subject, the initial values for these two-layered fits were taken to be the values obtained by the previous homogeneous fits at 10 mm and the linear fit of the tail of the reflectance at 30 mm for the first and second layer, respectively. The temporal range for the fit was from 20% of the maximum prior to the maximum peak, to 0.5% after the peak. Similar limits are found in the literature.[55]

The TPSFs measured with the apparatus were the convolutions of the TPSF due to the optical properties of the scattering medium with the instrument response function. Since each PMT had a characteristic response function, we measured each separately with a simple setup: the source and detector fibers faced each other and were separated by a thin piece of scattering paper to prevent PMT saturation and fill the whole numerical aperture of the detection fiber.[56] In the fitting procedure, each theoretical TPSF function of the medium was convolved with the experimental instrument response function (IRF) before comparison with the experimental TPSF. When IRF measurements are done well, this procedure avoids including a jitter delay time in the fitting parameters.

Finally, hemoglobin concentrations were recovered by inverting Eq. (9) for each layer of the model.

4 Results

4.1 Simulation of the Recovery Procedure

The fitting procedure was first tested on four simulated data sets with different values for the first and the second layer. These sets were generated using a 100 × 100 × 100 mm volume with 0.5 × 0.5 × 0.5 mm voxels. The thickness of the first layer was 10 mm, and the distance between the source and the detector was 30 mm. The simulations were made using a three-dimensional Monte Carlo code.[57] We simulated a peak amplitude of 10^4 photons, giving a photon noise of 1% at the peak, which is comparable to the experimental peak noise (<1%). Results in Table

1 show less than an 11.6% error on the recovery of the absorption coefficient of the first layer, and less than a 3.1% error for the second layer, by using the multi-distance fitting procedure. In these recoveries, we assumed that the thickness of the first layer was known. Table 1 shows that the linear fit of the tail of the TPSF logarithm gave a better estimate of the absorption coefficient than using a homogeneous model.

Separately, we simulated a complete Monte Carlo data set of 16 TPSFs, four source-detector distances (10, 15, 25, and 30 mm) for four different wavelengths (690, 750, 800, and 850 nm) with absorption coefficients computed from given hemoglobin concentrations in the superficial layer and in the brain. The concentrations chosen were 33 and 10 μ*M* in the superficial layer, and 65 and 22 μ*M* in the brain for HbO_2 and HbR, respectively. The thickness of the first layer was also 10 mm in these simulations. Recovered concentrations are shown in Fig. 1. Using the two-layered model, the errors in the recovered concentrations were less than 10% and 2% in the superficial layer and in the brain, respectively, when the thickness of the first layer was known. However, as shown in Fig. 1, the homogeneous model underestimated the hemoglobin concentrations in the brain by a factor of 30%.

4.2 Thickness Sensitivity

To test the sensitivity of the procedure to the thickness of the first layer, hemoglobin concentrations were recovered from the same simulated data set used in the previous section but assuming different thicknesses, between 8 and 12 mm, for the first layer. Errors in the HbO_2, HbR, and total hemoglobin (HbT) concentrations, and the oxygen saturation (SO_2) recovered with this procedure, are shown in Fig. 2. These results show that the accuracy of the recovery depends on the assumed thickness. For an error of ±1 mm, the errors in the recovered hemoglobin concentrations in the brain were between 10% and 15%. On the other hand, the SO_2 error stayed under 2%.

We also observed that the error in the hemoglobin concentrations in the brain due to an error in the estimation of the thickness of the first layer were always higher than the errors in the superficial layer. This was due to the brain's low contribution to the TPSFs for source-detector separations between 1 and 3 cm, so a small variation in the thickness resulted in a large relative variation in the brain's contribution to the TPSFs. This also explains the fact that underestimating the thickness of the superficial layer resulted in smaller errors for the hemoglobin concentration in the brain, as shown in Fig. 2, compared to an overestimation. However, when the thickness of the first layer was well estimated, the errors were similar in the superficial layers and in the brain.

Figure 2 also shows the sign of the error in the recovered concentrations. For an overestimation of the first-layer thickness, the contribution of the brain to the TPSF decreased, which resulted in an overestimation of the brain's hemoglobin to fit the theoretical model. As such, this overestimation produced an underestimation of hemoglobin in the superficial layer. On the other hand, if one underestimates the skin, skull, and CSF thicknesses, the contribution of the brain to the TPSF increases. This results in an underestimation of brain hemoglobin concentrations while superficial layers ones are less sensitive.

In practice, the thickness of the first layer enclosing skin, skull, and CSF can be determined very precisely using a high-resolution MRI scan. The error on the measurement is of the order of the voxel size. Here, the voxels were 1 mm^3 with a 3 T magnet, meaning that the maximum errors on the hemoglobin concentrations were expected to be no more than 15%.

4.3 In Vivo Measurements of Baseline Values

A typical example of the recovery procedure for *in vivo* data is presented in Fig. 3. The first step consisted of recovering the thickness of the model's first layer from an anatomical MRI image that comprised skin, skull, and CSF. After the fits were done with Eq. (1), the final step consisted of inverting Eq. (9) to recover hemoglobin concentrations. Detailed results for all subjects are presented in Table 2 for left-and right-side measurements on the forehead. For comparison, concentrations computed with absorption coefficients recovered with a homogeneous model are shown in Table 3. A group average was also performed with concentrations recovered using the two-layered model, and results are presented in Table 4.

5 Discussion

Table 2 and Table 4 show a clear distinction between the superficial layer and brain for hemoglobin baseline concentrations (as expected). This distinction is in agreement with results recovered using FD system (Choi et al.[8]). The HbO_2 and HbR concentrations were lower in the superficial layer than in the brain. The hemoglobin in the first layer was probably concentrated in the skin, which is highly irrigated with blood vessels; but this layer also included CSF, which contains low hemoglobin concentrations. However, our model did not validate this assumption. A three-layered model has been developed,[42] but to our knowledge, no results were reported. Our hemoglobin concentrations, computed with the homogeneous model, were overestimated in the superficial layer—as expected from the Monte Carlo simulation. However, the difference was lower for brain hemoglobin estimations, because the linear fit of the TPSF slopes gave a better estimate of the absorption coeffcient than the fit with the homogeneous analytical expression, as shown in Table 1. Our results suggest that the layered structure of the head should be taken into account to extract hemoglobin concentrations for the brain and to confirm the need for using a two-layered model.

We also observed a large intersubject variability for hemoglobin concentrations, shown in Table 2. This fact was also reported both in Choi et al.[8] and Comelli et al.,[26] thus rein-forcing the importance of baseline physiology measurements before interpreting activation maps of individual subjects. Simulation results from Table 2 and Fig. 2 show that the uncertainty in the estimated hemoglobin concentrations were less than 15% with our recovery procedure, which is due primarily to the estimation of the thickness of the superficial layer. This uncertainty alone cannot explain our observed variability between subjects. Differences in anatomical structure may explain this variability, but the subject's baseline metabolism at the moment of the experiment may also play a role. Physical activity, for example, just before the measurement raises the blood circulation in the body, which may alter the hemoglobin concentration of the brain tissue. Moreover, the two-layered model does not separate the CSF layer from the skin and skull, which can cause changes in light distribution. Also, the model assumes that all the boundaries are parallel and flat, which is obviously not the case in reality. Finally, other background absorbers can contribute to absorption, but their contributions are considered very low according to the literature.[32,50–52]

By looking at the SO_2 variations in the brain, we see in Table 2 that these variations are only 4% between subjects. This result was also reported in Choi et al. Figure 2 shows that the errors in the oxygen saturation are low (<2%) even if the assumption for the superficial layer thickness is bad. This makes sense, because the partial volume effect[5] reduces the magnitude of the estimated concentration. However, with a good choice of wavelengths, we can reduce the crosstalk and preserve the relative magnitudes for HbO_2 and HbR,[58] which gives good SO_2 values.

6 Conclusion

We reported baseline hemoglobin concentrations measured in human intra- and extracerebral tissue using a TD system with a two-layered analytical model for the first time. We showed that hemoglobin concentrations recovered with TD systems differ when a two-layered model is used instead of a homogeneous one. Clear distinctions were obtained between the superficial layer (skin+skull+CSF) and the brain. A large intersubject variability was observed, as previously reported in the literature. The uncertainty for hemoglobin concentrations was estimated to be less than 15% for simulations dominated by uncertainty in the layer thickness, suggesting that the observed difference between subjects was real.

Acknowledgments

L. Gagnon is supported by a postgraduate scholarship from the Natural Sciences and Engineering Council of Canada (NSERC). This work was supported by the National Institutes of Health grants P41-RR14075 and R01-EB002482 and the NSERC Discovery grant.

References

1. Villringer A, Hock C, Schleinkofer L, Dirnagl U. Near infrared spectroscopy (NIRS): a new tool to study hemodynamic changes during activation of brain function in human adults. Neurosci. Lett 1993;154:101–104. [PubMed: 8361619]
2. Hoshi Y, Tamura M. Multichannel near-infrared optical imaging of human brain activity. J. Appl. Physiol 1993;75:1842–1846. [PubMed: 8282640]
3. Obrig H, Villringer A. Beyond the visible—imaging the human brain with light. J. Cereb. Blood Flow Metab 2002;23:1–18. [PubMed: 12500086]
4. Gibson A, Hebden J, Arridge S. Recent advances in diffuse optical imaging. Phys. Med. Biol 2005;50:R1–R43. [PubMed: 15773619]
5. Boas D, Gaudette T, Strangman G, Cheng X, Marota J, Mandeville J. The Accuracy of near infrared spectroscopy and imaging during focal changes in cerebral hemodynamics. Neuroimage 2001;13:76–90. [PubMed: 11133311]
6. Franceschini M, Boas D. Noninvasive measurement of neuronal activity with near-infrared optical imaging. Neuroimage 2004;21:372–386. [PubMed: 14741675]
7. Fawzi YS, Youssef ABM, El-Batanony MH, Kadah YM. Determination of the optical properties of a two-layer tissue model by detecting photons migrating at progressively increasing depths. Appl. Opt 2003;42:6398–6410. [PubMed: 14649284]
8. Choi J, Wolf M, Toronov V, Wolf U, Polzonetti C, Hueber D, Safonova LP, Gupta R, Michalos A, Mantulin W, et al. Noninvasive determination of the optical properties of adult brain: near-infrared spectroscopy approach. J. Biomed. Opt 2004;9:221–229. [PubMed: 14715077]
9. Lim H, de Boer JF, Park BH, Lee EC, Yelin R, Yun SH. Optical frequency domain imaging with a rapidly swept laser in the 815–870 nm range. Opt. Express 2006;14:5937–5944. [PubMed: 19516763]
10. Li A, Kwong R, Cerussi A, Merritt S, Hayakawa C, Tromberg B. Method for recovering quantitative broadband diffuse optical spectra from layered media. Appl. Opt 2007;46:4828–4833. [PubMed: 17609733]
11. Wang RK, Wickramasinghe YA. Fast algorithm to determine optical properties of a turbid medium from time-resolved measurements. Appl. Opt 1998;37:7342–7351. [PubMed: 18301568]
12. Eda H, Oda I, Ito Y, Wada Y, Oikawa Y, Tsunazawa Y, Takada M, Tsuchiya Y, Yamashita Y, Oda M, et al. Multichannel time-resolved optical tomographic imaging system. Rev. Sci. Instrum 1999;70:3595–3602.
13. Schweiger M, Arridge S. Application of temporal filters to time resolved data in optical tomography. Phys. Med. Biol 1999;44:1699–1717. [PubMed: 10442707]
14. Pifferi A, Torricelli A, Taroni P, Cubeddu R. Reconstruction of absorber concentrations in a two-layer structure by use of multi-distance time-resolved reflectance spectroscopy. Opt. Lett 2001;26:1963–1965. [PubMed: 18059746]

15. Gao F, Tanikawa Y, Zhao H, Yamada Y. Semi-three-dimensional algorithm for time-resolved diffuse optical tomography by use of the generalized pulse spectrum technique. Appl. Opt 2002;41:7346–7358. [PubMed: 12477128]

16. Martelli F, Bianco SD, Zaccanti G, Pifferi A, Torricelli A, Bassi A, Taroni P, Cubeddu R. Phantom validation and in vivo application of an inversion procedure for retrieving the optical properties of diffusive layered media from time-resolved reflectance measurements. Opt. Lett 2004;29:2037–2039. [PubMed: 15455772]

17. Selb J, Stott J, Franceschini M, Sorenson A, Boas D. Improved sensitivity to cerebral hemodynamics during brain activation with a time-gated optical system: analytical model and experimental validation. J. Biomed. Opt 2005;10:011013.

18. Torricelli A, Pifferi A, Spinelli L, Cubeddu R, Martelli F, Bianco SD, Zaccanti G. Time-resolved reflectance at null source-detector separation: improving contrast and resolution in diffuse optical imaging. Phys. Rev. Lett 2005;95:078101. [PubMed: 16196825]

19. Selb J, Dale A, Boas D. Linear 3D reconstruction of time-domain diffuse optical imaging differential data: improved depth localization and lateral resolution. Opt. Express 2007;15:16400–16412. [PubMed: 19550930]

20. Swartling J, Dam J, Andersson-Engels S. Comparison of spatially and temporal resolved diffuse-reflectance measurements systems for determination of biomedical optical properties. Appl. Opt 2003;42:4612–4620. [PubMed: 12916630]

21. Liebert A, Wabnitz H, Grosenick D, Mller M, Macdonald R, Rinneberg H. Evaluation of optical properties of highly scattering media by moments of distribution of times of flight of photons. Appl. Opt 2003;42:5785–5790. [PubMed: 14528944]

22. Kienle A, Glanzmann T. *In vivo* determination of the optical properties of muscle with time-resolved reflectance using a layered model. Phys. Med. Biol 1999;44:2689–2702. [PubMed: 10588278]

23. Hoge RD, Franceschini MA, Covolan RJM, Huppert T, Mandeville JB, Boas DA. Simultaneous recording of task-induced changes in blood oxygenation, volume, and flow using diffuse optical imaging and arterial spin-labeling MRI. Neuroimage 2005;25:701–707. [PubMed: 15808971]

24. Hoge RD, Atkinson J, Gill B, Crelier GR, Marrett S, Pike GB. Investigation of BOLD signal dependence on cerebral blood flow and oxygen consumption:the deoxyhemoglobin dilution model. Magn. Reson. Med 1999;42:849–863. [PubMed: 10542343]

25. Yaroslavsky AN, Schulze PC, Yaroslavsky IV, Schober R, Ulrich F, Schwarzmaier H-J. Optical properties of selected native and coagulated human brain tissues *in vitro* in the visible and near infrared spectral range. Phys. Med. Biol 2002;47:2059–2073. [PubMed: 12118601]

26. Comelli D, Bassi A, Pifferi A, Taroni P, Torricelli A, Cubeddu R, Martelli F, Zaccanti G. *In vivo* time-resolved reflectance spectroscopy of the human forehead. Appl. Opt 2007;47:1717–1725. [PubMed: 17356614]

27. Contini D, Torricelli A, Pifferi A, Spinelli L, Paglia F, Cubeddu R. Multi-channel time-resolved system for functional near infrared spectroscopy. Opt. Express 2007;14:5418–5432. [PubMed: 19516708]

28. Saager RB, Berger AJ. Direct characterization and removal of interfering absorption trends in two-layer turbid media. J. Opt. Soc. Am. A 2005;22:1874–1882.

29. Leung TS, Elwell CE, Delpy DT. Estimation of cerebral oxy- and deoxy-haemoglobin concentration change in a layered adult head model using near-infrared spectroscopy and multivariate statistical analysis. Phys. Med. Biol 2005;50:5783–5798. [PubMed: 16333155]

30. Zhang Q, Brown EN, Stangman GE. Adaptative filtering for global interference cancellation and real-time recovery of evoked brain activity: a Monte Carlo simulation study. J. Biomed. Opt 2007;12:044014. [PubMed: 17867818]

31. Zhang Q, Brown EN, Stangman GE. Adaptative filtering to reduce global interference in evoked brain activity detection: a human subject case study. J. Biomed. Opt 2007;12:064009. [PubMed: 18163825]

32. Ohmae E, Oouchi Y, Oda M, Suzuki T, Nobesawa S, Kanno T, Yoshikawa E, Futatsubashi M, Ueda Y, Okada H, et al. Cerebral hemodynamics evaluation by near-infrared time-resolved spectroscopy: correlation with simultaneous positron emission tomography measurements. Neuroimage 2006;29:697–705. [PubMed: 16165372]

33. Kienle A, Patterson MS, Dognitz N, Bays R, Wagnieres G, van den Bergh H. Noninvasive determination of the optical properties of two-layered turbid media. Appl. Opt 1998;37:779–791. [PubMed: 18268653]
34. Kienle A, Glanzmann T, Wagnieres G, van den Bergh H. Investigation of two-layered turbid media with time-resolved reflectance. Appl. Opt 1998;37:6852–6862. [PubMed: 18301502]
35. Martelli F, Bianco SD, Zaccanti G. Procedure for retrieving the optical properties of a two-layered medium from time-resolved reflectance measurements. Opt. Lett 2003;28:1236–1238. [PubMed: 12885032]
36. Patterson MS, Chance B, Wilson C. Time resolved reflectance and transmittance for the noninvasive measurement of tissue optical properties. Appl. Opt 1989;28:2331–2336.
37. Schmittt JM, Zhou GX, Walker EC. Multilayer model of photon diffusion in skin. J. Opt. Soc. Am. A 1990;7:2141–2153. [PubMed: 2254803]
38. Dayan I, Havlin S, Weiss GH. Photon migration in a two-layer turbid medium. A diffusion analysis. J. Mod. Opt 1992;39:1567–1582.
39. Contini D, Martelli F, Zaccanti G. Photon migration through a turbid slab described by a model based on diffusion approximation. I. Theory. Appl. Opt 1997;36:4587–4599. [PubMed: 18259254]
40. Ripoll J, Ntziachristos V, Culver JP, Pattanayak DN, Yodh AG, Nieto-Vesperinas M. Recovery of optical parameters in multiple-layered diffusive media: theory and experiments. J. Opt. Soc. Am. A 2001;18:821–830.
41. Sassaroli A, Martelli F, Zaccanti G, Yamada Y. Performance of fitting procedures in curved geometry for retrieval of the optical properties of tissue from time-resolved measurements. Appl. Opt 2001;40:185–197. [PubMed: 18356990]
42. Martelli F, Sassaroli A, Yamada Y, Zaccanti G. Analytical approximate solutions of the time-domain diffusion equation in layered slabs. J. Opt. Soc. Am. A 2002;19:71–80.
43. Martelli F, Sassaroli A, Del-Bianco S, Yamada Y, Zaccanti G. Solution of the time-dependent diffusion equation for layered diffusive media by the eigenfucntion method. Phys. Rev. E 2003;67:056623.
44. Shendeleva ML. Time-domain Green functions for diffuse light in two adjoining turbid half-spaces. Appl. Opt 2007;46:1641–1649. [PubMed: 17356606]
45. Tualle JM, Nghiem HL, Ettori D, Sablong R, Tinet E, Avrillier S. Asymptotic behavior and inverse problem in layered scattering media. J. Opt. Soc. Am. A 2004;21:24–34.
46. Laidevant A, da Silva A, Berger M, Dinten J-M. Effects of the surface boundary on the determination of the optical properties of a turbid medium with time-resolved reflectance. Appl. Opt 2006;45:4756–4764. [PubMed: 16799691]
47. Shimada M, Hoshi Y, Yamada Y. Simple algorithm for the measurement of absorption coefficient of a two-layered medium by spatially resolved and time-resolved reflectance. Appl. Opt 2005;44:7554–7562. [PubMed: 16363780]
48. Kienle A, Patterson MS. Improved solutions of the steady-state and the time-resolved diffusion equations for reflectance from a semi-infinite turbid medium. J. Opt. Soc. Am. A 1997;14:246–254.
49. Golub GH, Welsch JH. Calculation of Gauss quadrature rules. Math. Comput 1969;23:221–230.
50. Tromberg BJ, Coquoz O, Fishkin JB, Pham T, Anderson E, Butler J, Cahn M, Gross JD, Venugopalan V, Pham D. Noninvasive measurements of breast tissue optical properties using frequency-domain photon migration. Philos. Trans. R. Soc. London, Ser. B 1997;352:661–668. [PubMed: 9232853]
51. Cope, M. Ph.D. thesis. University College London; 1991. The development of a near infrared spectroscopy system and its application for non invasive monitoring of cerebral blood and tissue oxygenation in the newborn infant.
52. Sevick EM, Chance B, Leigh J, Nioka S, Maris M. Quantitation of time- and frequency-resolved optical spectra for the determination of tissue oxygenation. Anal. Chem 2007;195:330–351.
53. Takatani S, Graham MD. Theoretical analysis of diffuse reflectance from a two-layer tissue model. IEEE Trans. Biomed. Eng 1979;26:656–664. [PubMed: 544437]
54. Hale GM, Querry MR. Optical constants of water in the 200 nm to 200 m wavelength region. Appl. Opt 1973;12:555–563.

55. Cubeddu R, Pifferi A, Taroni P, Torricelli A, Valentini G. Experimental test of theoretical models for time-resolved reflectance. Med. Phys 1996;23:1625–1633. [PubMed: 8892260]

56. Liebert A, Wabnitz H, Grosenick D, Macdonald R. Fiber dispersion in time domain measurements compromising the accuracy of determination of optical properties of strongly scattering media. J. Biomed. Opt 2003;8:512–516. [PubMed: 12880358]

57. Boas D, Culver J, Stott J, Dunn A. Three-dimensional Monte Carlo code for photon migration through complex heterogenous media including the adult human head. Opt. Express 2002;10:159–170. [PubMed: 19424345]

58. Strangman G, Franceschini MA, Boas DA. Factors affecting the accuracy of near-infrared spectroscopy concentration calculations for focal changes in oxygenation parameters. Neuroimage 2003;18:865–879. [PubMed: 12725763]

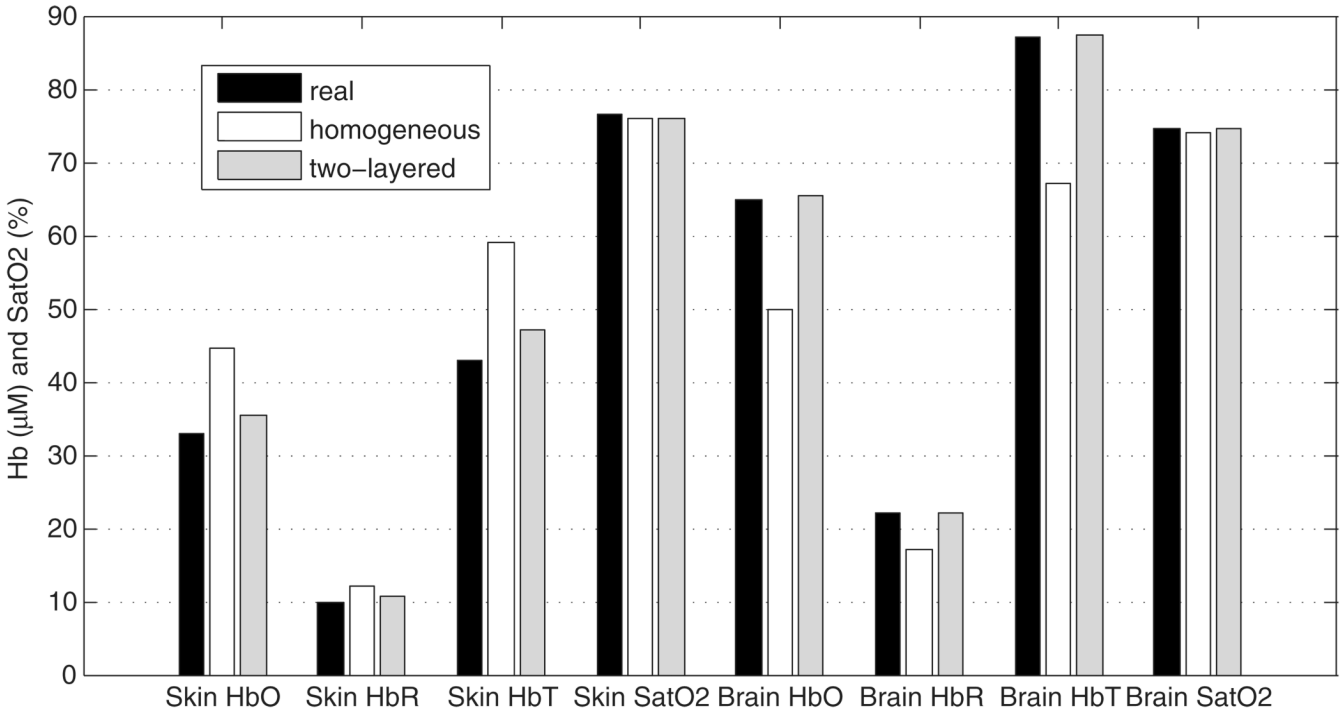

Fig. 1.

Hemoglobin concentrations and SO_2 recovered in the superficial layer and in the brain on simulated data.

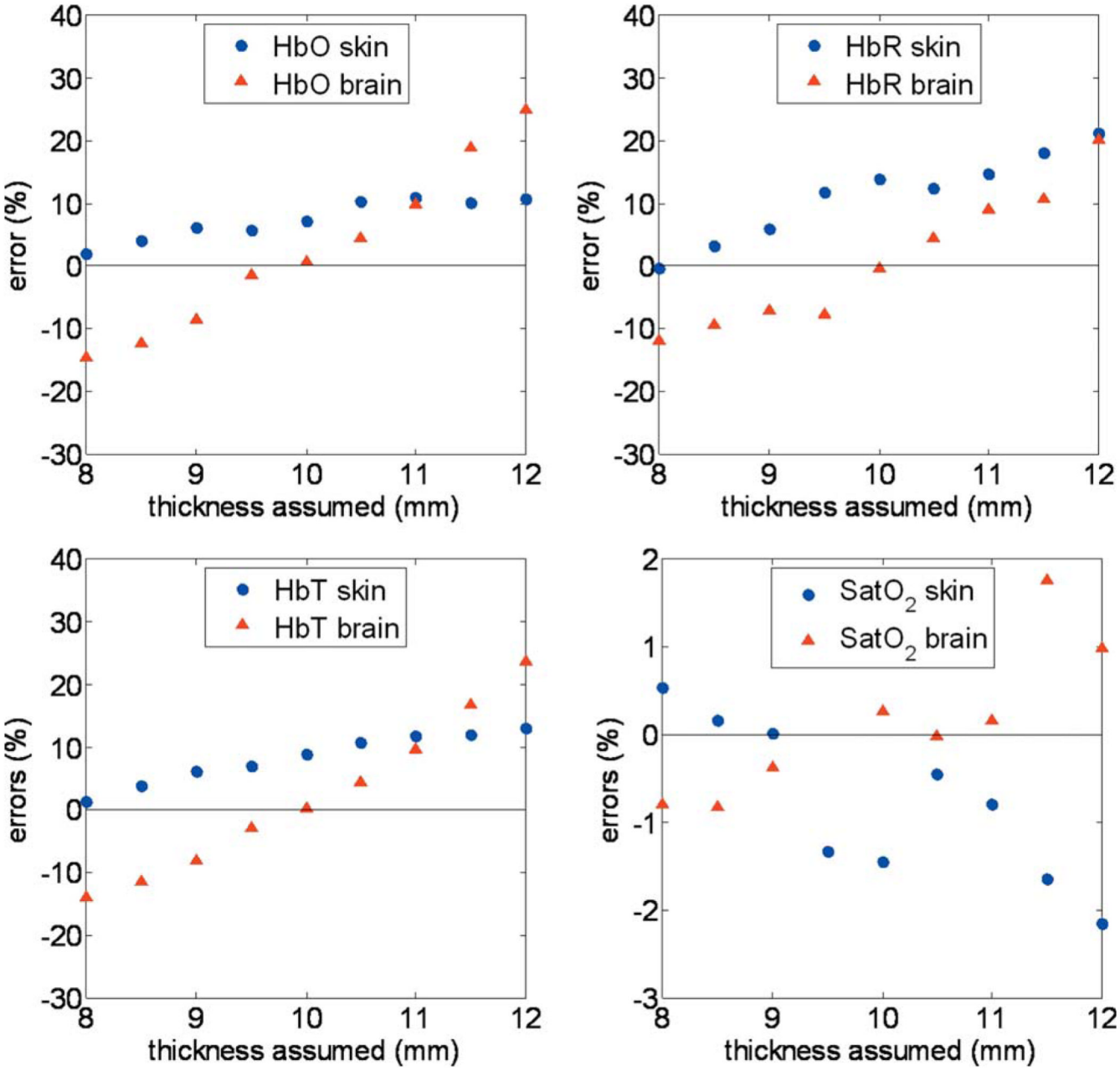

Fig. 2.

Errors on the recovered concentrations related to the assumed thickness of the first layer. HbO_2, HbR, HbT, and SO_2 errors are shown for data simulated with a first layer thickness of 10 mm.

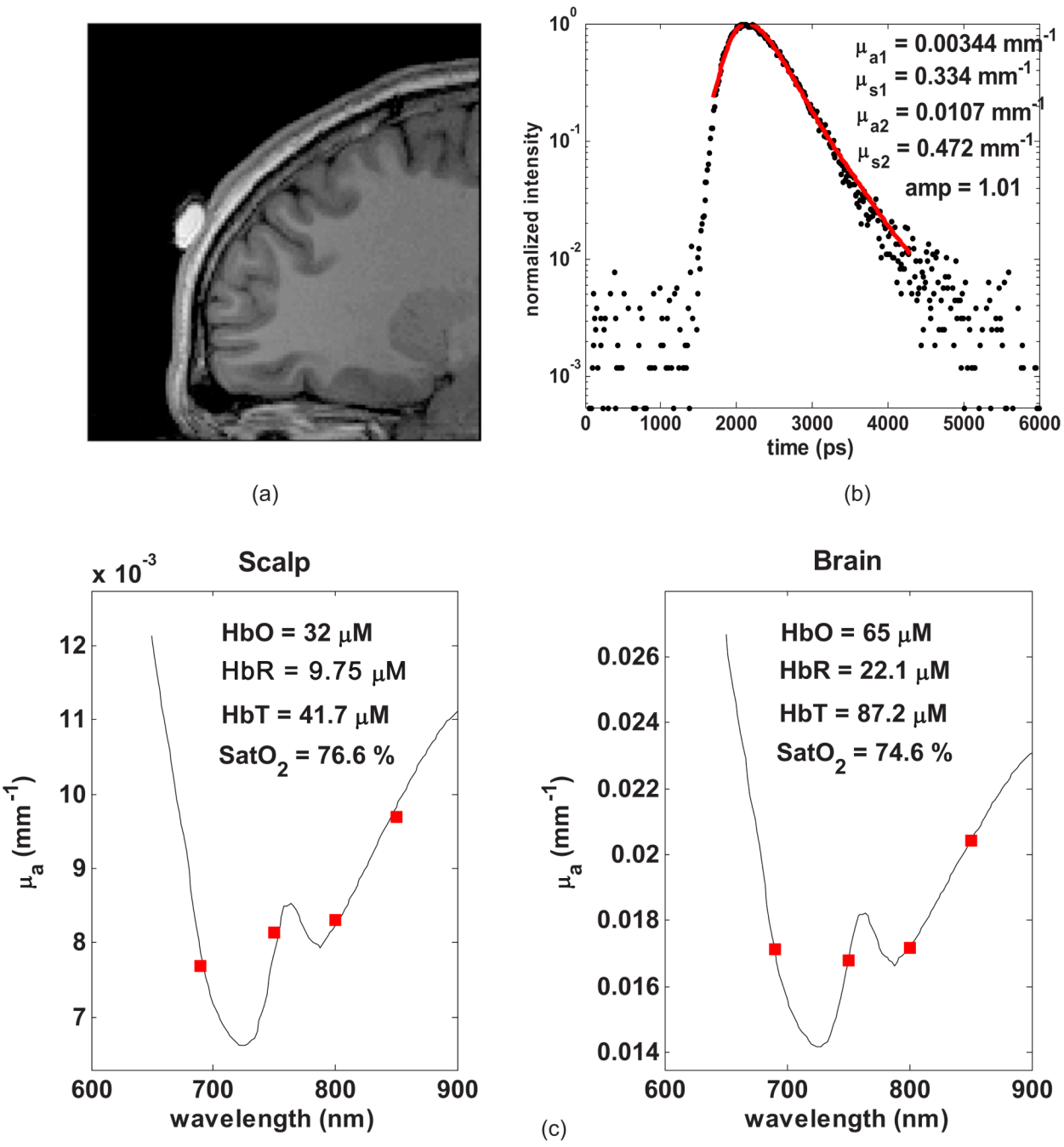

Fig. 3.

Typical procedure applied to recover the hemoglobin concentrations. (a) Recovery of the thickness of the first layer enclosing skin, scalp, and CSF on the MRI image. (b) Recovery of the reduced scattering and absorption coefficients for both layers using the fitting procedure. (c) Recovery of the chromophore concentrations with the inversion of Eq. (9).

Table 1

Absorption coefficients recovered with the two-layered model from four Monte Carlo data sets for both layers of the model. The thickness of the first layer was 10 mm. Absorption coefficients were recovered from a single TPSF with source-detector distances of 10 and 30 mm, and also from a multi-distance fit (10, 15, 25, and 30 mm). Results obtained using a homogeneous model are also shown for comparison.

	μ_{a1} (mm^{-1})			μ_{a2} (mm^{-1})			μ_a (mm^{-1})	
Data set	**Real**	**Recovered**	**Error (%)**	**Real**	**Recovered**	**Error (%)**	**Homogenous**	**Slope**
10 mm								
1	0.00809	0.0081	0.0894	0.0171	0.0154	9.53	0.0112	0.0204
2	0.00887	0.00807	9.01	0.0167	0.015	10.5	0.0112	0.0203
3	0.00849	0.00853	0.432	0.0172	0.0154	10.1	0.0117	0.0208
4	0.0101	0.0103	1.62	0.0204	0.0167	18.2	0.0137	0.0231
30 mm								
1	0.00809	0.00881	8.88	0.0171	0.0176	3.06	0.0132	0.0158
2	0.00887	0.00884	0.284	0.0167	0.0173	3.07	0.0131	0.0156
3	0.00849	0.00924	8.87	0.0172	0.0176	2.61	0.0135	0.016
4	0.0101	0.0108	6.45	0.0204	0.0214	5.11	0.0156	0.0181
4 TPSFs								
1	0.00809	0.00903	11.6	0.0171	0.0165	3.09		
2	0.00887	0.00889	0.228	0.0167	0.0164	1.93		
3	0.00849	0.0094	10.8	0.0172	0.0167	2.6		
4	0.0101	0.0108	6.34	0.0204	0.0201	1.44		

Table 2

Hemoglobin concentrations measured on the left and right hemisphere for each subject computed with absorption coefficients recovered using a two-layered model.

	HbO_2 (μM)		HbR (μM)		HbT (μM)		$S_{at}O_2$ (%)	
Subject	**Superficial**	**Brain**	**Superficial**	**Brain**	**Superficial**	**Brain**	**Superficial**	**Brain**
1 left (2 layers)	4.2	19.1	1.33	15.9	5.53	35	75.9	54.5
1 right (2 layers)	2.03	24.5	3.25	16.4	5.28	40.9	38.4	59.8
2 left (2 layers)	5.87	33.7	3.4	23	9.26	56.7	63.3	59.5
2 right (2 layers)	4.35	32.7	4.26	20.5	8.6	53.2	50.5	61.5
3 left (2 layers)	15.9	39.6	11.1	21.8	27	61.4	58.9	63.7
3 right (2 layers)	17.7	43.4	11.8	20	29.6	63.4	60	68.4
4 left (2 layers)	27.1	35.6	13.9	26.4	41	62	66.1	57.4
4 right (2 layers)	25.8	36.7	13.9	22.7	39.7	59.4	65.1	61.8
5 left (2 layers)	10.4	21.2	5.48	17	15.9	38.2	65.4	55.4
5 right (2 layers)	12.7	23.7	4.49	15.3	17.2	39	73.9	60.8

Table 3

Hemoglobin concentrations measured on the left and right hemisphere for each subject computed with absorption coefficients recovered using a homogeneous model for the superficial layer and the linear fit of the TPSF slope for the brain. Superficial layer concentrations correspond to measurements at 10 mm, while brain concentrations correspond to measurements at 30 mm.

	HbO_2 (μM)		HbR (μM)		HbT (μM)		SO_2 (%)	
Subject	**Superficial**	**Brain**	**Superficial**	**Brain**	**Superficial**	**Brain**	**Superficial**	**Brain**
1 left (1 layer)	8.08	22.5	3.14	17.6	11.2	40.1	72	56.1
1 right (1 layer)	15.3	24.4	5.68	17.2	21	41.7	72.9	58.7
2 left (1 layer)	22.9	31.5	5.99	18.7	28.9	50.1	79.3	62.8
2 right (1 layer)	19.9	31.6	7.7	17	27.6	48.6	72.1	64.9
3 left (1 layer)	19.2	16.9	8.28	25.9	27.5	42.8	69.9	39.6
3 right (1 layer)	28	31.6	13.4	22.4	41.4	54	67.7	58.5
4 left (1 layer)	19.2	33.9	11.9	17.7	31.2	51.6	61.7	65.7
4 right (1 layer)	23.8	39.7	21.7	18.3	45.4	58	52.3	68.5
5 left (1 layer)	12	24.8	10.1	18.8	22.2	43.6	54.2	56.8
5 right (1 layer)	12.2	25.9	7.87	17.2	20.1	43.1	60.8	60

Table 4

Average hemoglobin concentrations for all the subjects. Concentrations were computed using the two-layered model.

	Left		Right		Average	
Chromophore	**Superficial**	**Brain**	**Superficial**	**Brain**	**Superficial**	**Brain**
HbO_2	12.7	29.8	12.5	32.2	12.6	31
(μM)	±9.25	±9.12	±9.77	±8.31	±8.97	±8.32
HbR	7.05	20.8	7.54	19	7.29	19.9
(μM)	±5.3	±4.34	±4.92	±3.05	±4.83	±3.67
HbT	19.7	50.7	20.1	51.2	19.9	50.9
(μM)	±14.4	±13	±14.4	±10.9	±13.6	±11.3
SO_2	65.9	58.1	57.6	62.5	61.7	60.3
(%)	±6.24	±3.66	±13.6	±3.43	±10.9	±4.06